

Phase diagrams and critical behavior of a two-dimensional anisotropic Heisenberg antiferromagnet

D. P. Landau

Department of Physics and Astronomy, University of Georgia, Athens, Georgia 30602

K. Binder

Institut für Festkörperforschung, KFA Jülich, Postfach 1913, D5170-Jülich, West Germany

(Received 9 March 1981)

A classical $d=2$ anisotropic Heisenberg antiferromagnet is studied in the presence of a uniform magnetic field (H) along the easy axis. Ground-state properties are determined exactly, and expected low-temperature behavior is calculated for the antiferromagnetic state using first-order spin-wave theory and for the spin-flop state using a modification of the harmonic approximation used by Berezinski for the classical XY model. Extensive data are obtained from Monte Carlo simulations on $L \times L$ square lattices with periodic boundary conditions and nearest-neighbor coupling $J_{\perp}/J_{\parallel}=0.8$. The phase diagram agrees with the predictions of renormalization-group theory: The antiferromagnetic state is Ising-like, and the spin-flop phase shows behavior similar to the two-dimensional XY model and the two-dimensional isotropic Heisenberg model in a field. However, the existence of biconical or bicritical points at finite temperature could not be confirmed. Spin-wave theory and the modified harmonic-approximation theory for the spin-flop state are valid only at extremely low temperatures.

I. INTRODUCTION

The moderately anisotropic Heisenberg model is a simple example of a system which exhibits bicritical behavior¹⁻³ and which provides a useful starting point for understanding the behavior of physical systems. The simplest (uniaxial) form of the model is

$$\mathcal{H} = J \sum_{(ij)} [(1 - \Delta)(s_{ix}s_{jx} + s_{iy}s_{jy}) + s_{iz}s_{jz}] + H_{\parallel} \sum_i s_{iz} \quad (1)$$

where \bar{s}_i is a unit vector in the direction of the classical magnetic moment at site i , Δ is the uniaxial anisotropy, and the sum (ij) is over all nearest-neighbor pairs. The behavior of this model has been studied in detail using mean-field theory⁴⁻⁶ and in three dimensions using renormalization-group theory^{1,2,7-9} and Monte Carlo computer simulations.³ The studies showed that the low-temperature, low-field ordered state is a two sublattice antiferromagnet (AF) which is separated from the paramagnetic state (P) by a line of second-order phase transitions. Only the z component of the fluctuations becomes critical along this line and the critical exponents are thus the same as a system with spin dimensionality $n=1$ (Ising). At sufficiently low temperatures the system undergoes a first-order transition to a canted "spin-flop" state (SF) as the field is increased. The SF state is separated from the P phase by a line of second-order transitions which are characterized by

$n=2$ (XY -model) exponents. The point at which the AF and P phases become simultaneously critical is termed the "bicritical point" and has critical behavior described by Heisenberg ($n=3$) exponents in three-dimensional systems [see Fig. 1(a)].

In this paper we shall consider the behavior of the anisotropic Heisenberg model in two dimensions. General arguments would lead us to expect that the spin-flop phase should behave like a two-dimensional XY model ($n=2$) and thus show no long-range order.¹⁰ This model is likely to correspond most closely to a physical magnetic system capable of exhibiting two-dimensional XY -like behavior since it requires only that the system be quasi-two dimensional with negligible coupling between different layers. A realization of a true XY (or plane rotator) model would occur only if the single ion uniaxial coupling or anisotropic exchange were sufficiently¹⁴ large and of the right sign in addition. Possible physical realization of this model are the antiferromagnetic layer compounds¹¹ of the type $(\text{CH}_2)_n(\text{NH}_3)_2\text{MnCl}_4$.

The behavior of this model in the region where the AF and SF phases "meet" is not clear in two dimensions. If a simple bicritical point occurs, it would be expected to have the character of a two-dimensional Heisenberg model which is now believed to be at $T=0$. In this case the phase diagram looks like Fig. 1(b) instead of Fig. 1(a). An ϵ -expansion renormalization-group calculation indicates that a new tetracritical biconical point is stable in systems with spin dimensionality $n > n^* \sim 2.8$ for $d=2$. If this es-

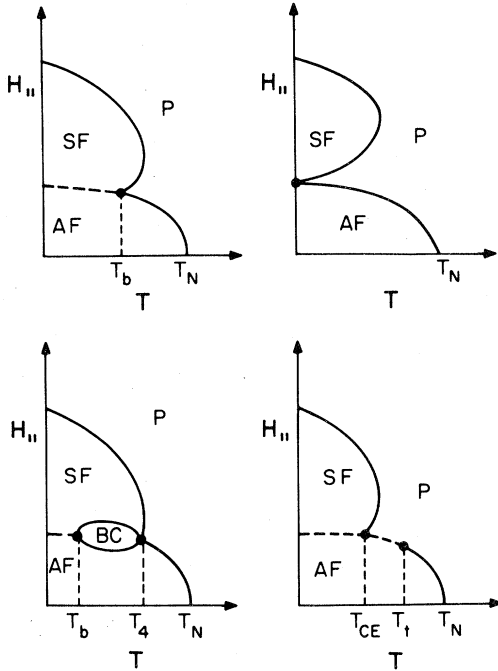


FIG. 1. Possible phase diagrams in the $H_{||}T$ plane. Second-order boundaries are shown by solid curves and first-order boundaries by dashed lines. The phases shown are denoted by: AF—antiferromagnetic; P—paramagnetic; SF—spin flop; BC—biconical. (a) A bicritical point occurs at T_b ; (b) a bicritical point is at $T=0$; (c) a biconical tetracritical point appears at T_4 and a bicritical point occurs at T_b ; and (d) a tricritical point appears at T_t and a critical end point at T_{cE} .

time for n^x is accurate we would expect that the phase diagram should look like Fig. 1(c), where the bicritical point T_b could be at $T=0$. (We ignore here the decoupled tetracritical point which is expected to be valid only for $n > 11$.) Another possible phase diagram is shown in Fig. 1(d); such behavior is in fact predicted by mean-field theory⁴ but only if in-

trasublattice (e.g., next-nearest-neighbor) coupling is included.

In this paper we shall present results of extensive Monte Carlo calculations which can be used to determine the phase boundary and to test some of the above predictions. In Sec. II we shall describe theoretical calculations appropriate to the low-temperature region. Section III provides information about the simulation techniques used. In Sec. IV we shall present simulation results which will then be analyzed and compared with theory.

II. THEORETICAL BACKGROUND

At $T=0$ this classical model can be solved exactly.³ The energy of the paramagnetic state is

$$\mathcal{H}_P = \frac{1}{2} NqJ(1 - 2h_{||}) \quad (2)$$

where $h_{||} = H_{||}/qJ$, and q is the coordination number; and for the antiferromagnetic state

$$\mathcal{H}_{AF} = -\frac{1}{2} NqJ \quad (3)$$

For the spin-flop state the energy is

$$\mathcal{H}_{SF} = -\frac{1}{2} NqJ \left(1 - \Delta + \frac{h_{||}^2}{2 - \Delta} \right) \quad (4)$$

By comparing these energies we find that the $AF \rightarrow SF$ transition occurs at a critical field

$$h_{c1} = [\Delta(2 - \Delta)]^{1/2} \quad (5)$$

and the $SF \rightarrow P$ transition at

$$h_{c2} = 2 - \Delta \quad (6)$$

For the AF phase we can use first-order spin-wave theory³ to study the temperature dependence of the bulk properties. We find that the magnetizations of the two sublattices are

$$m_I = 1 - \frac{kT}{qJ} \left(\frac{1 - h_{||}}{1 + h_{||}} \right)^{1/2} \frac{1}{N} \sum_{\vec{k}} \frac{1}{(1 - h_{||}^2)^{1/2} - (1 - \Delta)\gamma(\vec{k})} \quad (7a)$$

$$m_{II} = -1 + \frac{kT}{qJ} \left(\frac{1 + h_{||}}{1 - h_{||}} \right)^{1/2} \frac{1}{N} \sum_{\vec{k}} \frac{1}{(1 - h_{||}^2)^{1/2} - (1 - \Delta)\gamma(\vec{k})} \quad (7b)$$

where

$$\gamma(\vec{k}) = \frac{1}{q} \sum_{\substack{NN \text{ pairs} \\ (ij)}} e^{i\vec{k} \cdot \vec{r}_{ij}} \quad (8)$$

The reduced magnetization M and sublattice magnetization m are then

$$M = \frac{1}{2} (m_I + m_{II}) \quad (9a)$$

$$m = \frac{1}{2} (m_I - m_{II}) \quad (9b)$$

From Eqs. (8) and (9) we find

$$M_{||}/h_{||}(1 - m_{II}) = 1 \quad (10)$$

i.e., the ratio is independent of T , $H_{||}$, and L within the context of first-order spin-wave theory.

The treatment of the SF phase is more complicated than that of the AF state. In particular, if the state does behave like a two-dimensional XY model, there is no long-range order and spin-wave theory is inad-

quate. We can, however, adapt the harmonic approximation¹² used for the plane rotator in the following way. We first transform the spin components into polar coordinates:

$$s_{iz} = \cos\theta_i, \quad (11a)$$

$$s_{ix} = \sin\theta_i \cos\phi_i, \quad (11b)$$

$$s_{iy} = \sin\theta_i \sin\phi_i, \quad i \in \text{sublattice 1}, \quad (11c)$$

and

$$s_{iz} = \cos\theta_i, \quad (12a)$$

$$s_{ix} = -\sin\theta_i \cos\phi_i, \quad (12b)$$

$$s_{iy} = \sin\theta_i \sin\phi_i, \quad i \in \text{sublattice 2}. \quad (12c)$$

The Hamiltonian [Eq. (1)] may then be rewritten

$$\mathcal{H} = -J \sum_{(ij)} [(1-\Delta) \sin\theta_i \sin\theta_j \cos(\phi_i - \phi_j) - \cos\theta_i \cos\theta_j] - H_{\parallel} \sum_i \cos\theta_i. \quad (13)$$

$$\mathcal{H}_0 = -\frac{1}{2} NqJ [(1-\Delta) + (2-\Delta) \cos^2\theta], \quad (16a)$$

$$\mathcal{H}_1 = J(1-\Delta) [1 - (h/h_{c2})^2] \frac{1}{2} \sum_{(i,j)} (\phi_i - \phi_j)^2, \quad (16b)$$

$$\mathcal{H}_2 = -\frac{1}{2} qJ(1-\Delta) \sum_i (\theta_i - \theta)^2 - J \sum_{(i,j)} [(1-\Delta) \cos^2\theta + \sin^2\theta] (\theta_i - \theta) (\theta_j - \theta). \quad (16c)$$

Note that in this approximation the fluctuations in the longitudinal degrees of freedom $\{\theta_i\}$ and the transverse ones $\{\phi_i\}$ are not coupled. Hence, Eq. (16b) just corresponds to a planar model with modified exchange constant

$$J' = J(1-\Delta) [1 - (h/h_{c2})^2] \quad (17)$$

and

$$kT_c/J' = \text{const} = kT_c^{\text{KT}} / \{J(1-\Delta) [1 - (h/h_{c2})^2]\}, \quad (18)$$

where T_c^{KT} is the critical temperature of the planar model of Kosterlitz and Thouless.¹⁷

This expression cannot be correct for small fields since it shows no instability at the lower critical field h_{c1} . Using Eqs. (15) and (16) we find that the free energy in the limit of large fields can be approximated by

$$f = -kT \ln \sin\theta - \frac{1}{2} qJ [(1-\Delta) + (2-\Delta) \cos^2\theta] + f_{pl} \{J(1-\Delta) (1 - h^2/h_{c2}^2)\} + f_{pl} \{J(1-\Delta)\}, \quad (19)$$

where $f_{pl}\{J'\}$ is the free energy of the planar model with coupling J' . From the work of Berezinski¹² we find

$$f_{pl}\{J'\} = -kT \ln \text{const} + \frac{1}{2} kT \ln(2\pi J'/kT) \quad (20)$$

and since the appearance of the spin-flop state at $T=0$ means that

$$\ln \sin\theta = \frac{1}{2} \ln(1 - h^2/h_{c2}^2) \quad (21)$$

The SF ground state obtained from Eq. (13) has $\phi_i=0$, $\theta_i = \cos^{-1}\{H_{\parallel}/[qJ(2-\Delta)]\}$. If we then expand up to quadratic terms:

$$\cos(\phi_i - \phi_j) = 1 - \frac{1}{2} (\phi_i - \phi_j)^2 + \dots, \quad (14a)$$

$$\cos\theta_i = \cos\theta - \sin\theta(\theta_i - \theta) - \frac{1}{2} \cos\theta(\theta_i - \theta)^2 + \dots, \quad (14b)$$

$$\sin\theta_i = \sin\theta + \cos\theta(\theta_i - \theta) - \frac{1}{2} \sin\theta(\theta_i - \theta)^2 + \dots, \quad (14c)$$

and insert these expressions into Eq. (13) we find that keeping only terms of second order the Hamiltonian becomes

$$\mathcal{H} = \mathcal{H}_0 + \mathcal{H}_1(\{\phi_i\}) + \mathcal{H}_2(\{\theta_i\}), \quad (15)$$

where

we can rewrite Eq. (19)

$$f = -\frac{1}{2} qJ [(1-\Delta) + (2-\Delta) h^2/h_{c2}^2] - 2kT \ln \text{const} + kT \ln[2\pi J(1-\Delta)/kT]. \quad (22)$$

From Eq. (22) we see that the term which is linear in T is independent of h . This means that the magnetization and susceptibility will have a temperature dependence determined by terms of order T^2 and

higher:

$$M = h/h_{c2} + O(T^2) , \quad (23a)$$

$$\chi = \frac{1}{4J(2-\Delta)} + O(T^2) . \quad (23b)$$

The thermal properties are then given by

$$S = -k \ln \left[\frac{2\pi J(1-\Delta)}{kT} \right] + 2k \ln \text{const} - k , \quad (24a)$$

$$U = -\frac{qJ}{2} \left[(1-\Delta) + (2-\Delta) \frac{h^2}{h_{c2}^2} \right] + kT , \quad (24b)$$

$$C = k . \quad (24c)$$

III. MONTE CARLO BACKGROUND

In the simulations we generate a Markov chain of spin configurations using a set of transition probabilities which satisfy the conditions of detailed balance. We have studied $L \times L$ square lattices with periodic boundary conditions. The initial spin configuration is varied in order to allow investigation of possible metastable states and relaxation effects. Each lattice site is considered in turn and given the opportunity to "flip" to a new randomly chosen orientation with a corresponding change in the energy of the system of ΔE . If $e^{-\Delta E/kT}$ exceeds a random number p in the interval $0 < p < 1$, the change is carried out; otherwise it is rejected. One Monte Carlo step per spin (MCS) corresponds to the "time" required to consider each lattice site once. In order to reduce the computing time required, the same procedure is carried out simultaneously using the same random numbers for four lattices with different values of field and temperature. At very low temperatures this procedure is inefficient since most randomly chosen new spin directions involve an amount of energy ΔE which is large compared to kT . For very low-temperature studies we then modified the algorithm to allow a spin \vec{S}_i attempt to flip to a new position \vec{S}'_i which lies within a cone about the original direction, i.e.,

$$S'_{i\alpha} = \frac{S_{i\alpha} + \Delta \xi_{\alpha}}{\left[\sum_{\alpha} (S_{i\alpha} + \Delta \xi_{\alpha})^2 \right]^{1/2}} , \quad (25)$$

where α refers to the Cartesian spin component, ξ_{α} is a random number lying between -1 and $+1$ and is chosen separately for determining each spin component, and Δ limits the maximum possible change. In practice we choose $\Delta = 0.5T$. The method is described in more detail elsewhere.^{13,14} Quantities such as the internal energy E , magnetization M , and order parameter m are determined directly from the average of these quantities over many spin configura-

tions. For example, the order parameter is given by

$$m_{\parallel} = \frac{1}{L^2} \left\langle \left(\sum_i S_{iz} e^{-i \vec{k}_0 \cdot \vec{R}_i} \right)^2 \right\rangle^{1/2} , \quad (26a)$$

$$m_{\perp} = \frac{1}{L^2} \left\langle \left(\sum_i S_{ix} e^{-i \vec{k}_0 \cdot \vec{R}_i} \right)^2 + \left(\sum_i S_{iy} e^{-i \vec{k}_0 \cdot \vec{R}_i} \right)^2 \right\rangle^{1/2} , \quad (26b)$$

where \vec{k}_0 describes the periodicity of the antiferromagnetic ground state and the angle brackets denote averages. Fluctuations in the bulk properties are used to determine thermodynamic response functions

$$\frac{C}{k} = \left[\frac{L^2}{T^2} \right] (\langle E^2 \rangle - \langle E \rangle^2) , \quad (27a)$$

$$\chi_{\parallel} = \left[\frac{L^2}{T} \right] (\langle M_{\parallel}^2 \rangle - \langle M \rangle_{\parallel}^2) , \quad (27b)$$

$$\chi_{\parallel}^{\dagger} = \left[\frac{L^2}{T} \right] \langle m_{\parallel}^2 \rangle , \quad (27c)$$

$$\chi_{\perp}^{\dagger} = \frac{L^2}{T} \langle m_{\perp}^2 \rangle . \quad (27d)$$

IV. RESULTS AND DISCUSSION

A. Results in the $H_{\parallel}T$ plane

1. Antiferromagnetic state

The behavior of the antiferromagnetic (AF) phase and the transition to the paramagnetic (P) state were studied along paths of constant field and along paths where H_{\parallel}/T was held fixed. Typical runs were made by averaging over 400 MCS obtained for a given starting configuration and then repeating the calculation using one or two additional starting configurations. In order to study the zero-field critical behavior, however, it was necessary to average over at least 2000 MCS in the vicinity of the transition. Data for the order parameter (staggered magnetization) are shown in Fig. 2 for three paths of constant field. The behavior is qualitatively similar in all three cases. At low temperature the order parameter falls off slowly with temperature in agreement with first-order spin-wave theory. However, the decrease in the order parameter with increasing temperature quickly becomes much more rapid than the spin-wave prediction. At higher temperatures still the order parameter shows a rapid dropoff for all lattice sizes, indicative of a phase transition to the paramagnetic state; the ratio of T_c at which the transition occurs

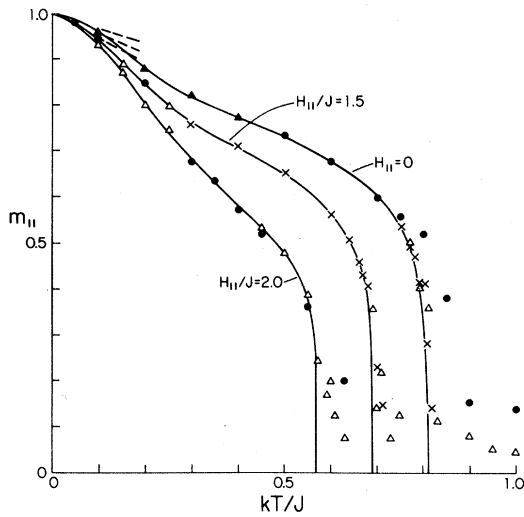


FIG. 2. Temperature dependence of the antiferromagnetic order parameter along paths of constant field. Data are shown for $L = 20$ (\bullet); $L = 40$ (Δ); $L = 100$ (\times). Solid curves show the estimated infinite lattice behavior. The dashed lines show the low-temperature spin-wave predictions for $L = 40$.

decreases monotonically as the field increases. Above the transition the finite system size gives rise to a short-range-order "tail" which decreases with increasing system size. The variation of the internal energy with temperature is shown in Fig. 3 for the same three paths of constant field. The low-temperature behavior of the internal energy is virtually identical for all three paths. Here too the prediction of first-order spin-wave theory is valid only at extremely low temperature. Inflection points appear at $T_c(H)$ but the curves show no dramatic features.

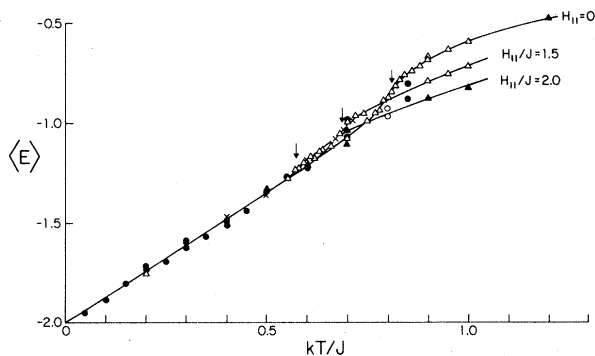


FIG. 3. Temperature dependence of the internal energy along paths of constant field. Data are shown for $L = 10$ (\blacktriangle); $L = 20$ (\bullet); $L = 40$ (Δ); $L = 100$ (\times). The solid curves show the infinite lattice behavior. The dashed line shows the prediction of first-order spin-wave theory for $L = 40$. Arrows indicate our estimates for $T_c(H)$.

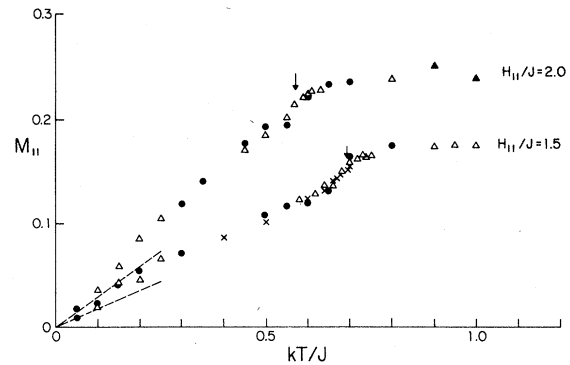


FIG. 4. Temperature dependence of the magnetization along paths of constant field. Data are shown for $L = 10$ (\blacktriangle); $L = 20$ (\bullet); $L = 40$ (Δ); $L = 100$ (\times). The dashed lines show the predictions of first-order spin-wave theory for $L = 40$. Arrows indicate our estimates for $T_c(H)$.

Results for the magnetization along constant field paths are shown in Fig. 4. Again first-order spin-wave theory is sufficient only at very low temperatures; the transition is marked by inflection points. Finite-size effects are not marked for either the internal energy or the magnetization.

In Fig. 5 we test this spin-wave relation given in Eq. (10) for three field values. Although the data do all apparently lie upon a single curve, they do show deviations from the prediction even at low temperatures.

The critical behavior in zero applied field is examined in Fig. 6. The asymptotic behavior of the order parameter is well described by the Ising exponent $\beta = \frac{1}{8}$ and a critical amplitude $B = 0.75$. Farther away from T_c the order parameter deviates above the asymptotic form. Fluctuations in the high-temperature ordering susceptibility were quite pronounced. Outside a region very close to T_c where finite-size effects were pronounced, the data are quite consistent with the Ising exponent $\gamma = \frac{7}{4}$ with a criti-

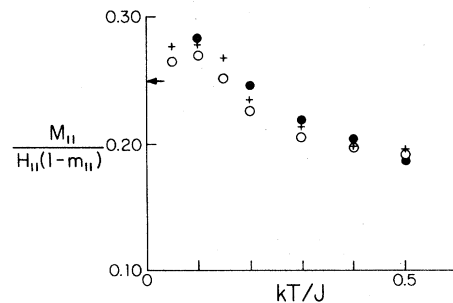


FIG. 5. Low-temperature behavior of the antiferromagnetic state. Data are for $H/J = 0.5$ (\bullet); $H/J = 1.0$ ($+$); $H/J = 1.5$ (\circ). The arrow shows the spin-wave asymptote.

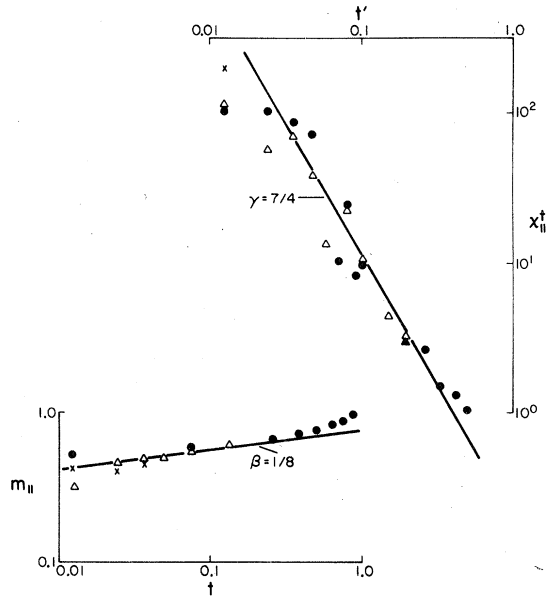


FIG. 6. Zero-field critical behavior of the order parameter and high-temperature ordering susceptibility. Data are for $L = 20$ (\bullet); $L = 40$ (Δ); $L = 100$ (\times). $t = (1 - T/T_c)$ and $t' = (1 - T_c/T)$.

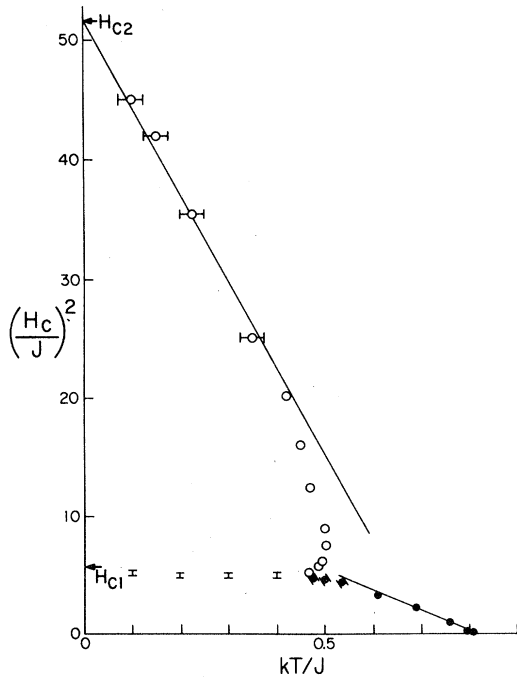


FIG. 7. Phase diagram in the $H_{||} - T$ plane. Closed circles show the AF \rightarrow P transition and open circles the SF \rightarrow P transition. The solid lines show fits to asymptotic high-field and low-field behavior.

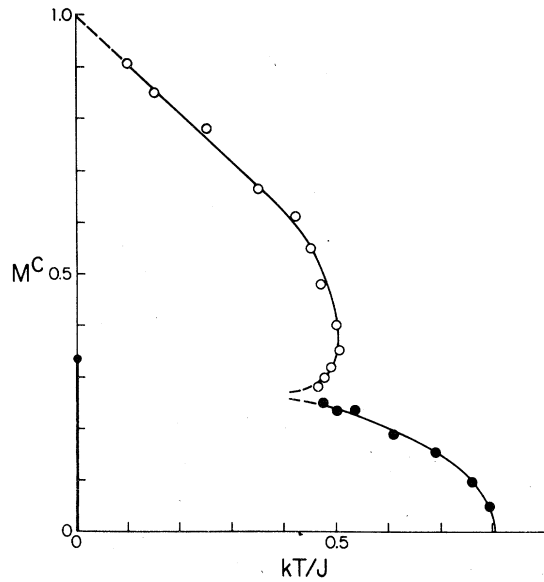


FIG. 8. Temperature dependence of the critical magnetization $M_{||}^c$.

cal amplitude of $C^+ = 0.2$. When a small uniform field is added the Ising exponents continue to provide an adequate description of the critical behavior, but as the field increases the order-parameter amplitude goes down and the susceptibility amplitude gets larger. The variation of the critical temperature with applied uniform magnetic field is shown in Fig. 7. The low-field variation is well described by

$$H_c^2 \propto [T_c(H=0) - T_c(H)] \quad (28)$$

The corresponding values of the critical magnetization M^c at the AF \rightarrow P phase boundary are shown in Fig. 8.

2. Spin-flop state

The properties of the spin-flop state and the transitions to the paramagnetic state were studied along paths of constant field. The transverse order parameter showed substantial fluctuations and decreased steadily with increasing lattice size even at low temperatures. We interpret this behavior as indicating the absence of long-range order in the thermodynamic limit. Since order in the spin-flop state is described by a two-component order parameter, simple universality arguments suggest that the SF state belongs to the universality class of the XY model. Since the two-dimensional XY model does not show long-range order the observed behavior is no surprise. The temperature dependence of the internal energy for two field values is shown in Fig. 9. The low-temperature behavior is well described by the harmonic approximation prediction of Eq. (24). The data show only a

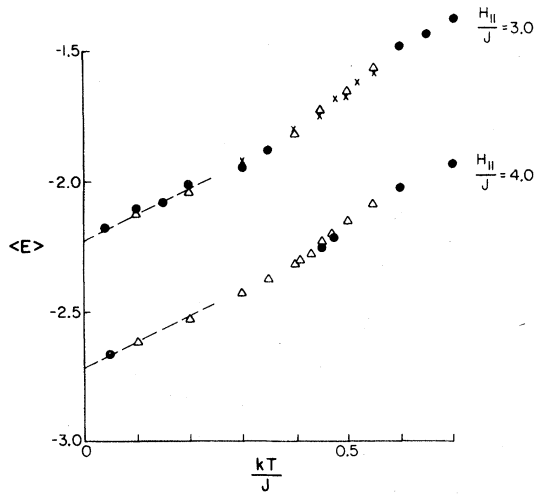


FIG. 9. Temperature dependence of the internal energy for the SF state along paths of constant field. Data are for $L = 20$ (\bullet); $L = 40$ (Δ); $L = 100$ (X). The dashed lines show the low-temperature theoretical prediction of Eq. (24).

slight increase in slope at higher temperatures suggesting that the specific heat is nondivergent. The magnetization shows essentially no effect at all at the phase boundary [as shown in Fig. 10(a)]. A careful study of the low-temperature behavior of the magnetization shows that deviations from the predicted constant value [see Eq. (24)] occur rapidly. We have also investigated other properties of the spin-flop state to see if they are consistent with the harmonic

approximation. Equilibrium spin configurations were examined for indications of vortex behavior in the XY plane. In Fig. 11 we show the projection of the spin onto the XY plane of a 20×20 section of a $L = 40$ lattice with $H/J = 4.0$ and $kT/J = 0.3$. This figure shows substantial spin-wave "noise" with no obvious vortexlike behavior. We have adopted a procedure suggested to us by Thouless,¹⁵ and since used by Chester and Tobochnik,¹⁶ to analyze the spin state for vortices. The vorticity in a given region is determined by traveling around a closed loop (in practice a square of nearest-neighbor sites) and adding the relative angular difference between spin directions around the loop. A net difference of 0 indicates no vorticity whereas net differences of $+2\pi$ and -2π indicate positive and negative (anti) vorticity, respectively. Since the nearest-neighbor interaction is antiferromagnetic it was necessary to add a phase angle of π to successive corners. The small circle shown in Fig. 11 is the center of a vortex-antivortex pair which is easily located using this prescription. Figure 12 shows the change in vortex behavior with increasing temperature: the number of vortices rapidly goes up and in addition to pairs larger clusters begin to form. Eventually the vortex pairs begin to unbind as the number of vortices continues to increase. According to the Kosterlitz-Thouless theory¹⁷ this unbinding signals the phase transition. The theory also predicts that the low-temperature density of vortex pairs ρ is given by

$$\rho = R \exp(-2\mu/kT) , \quad (29)$$

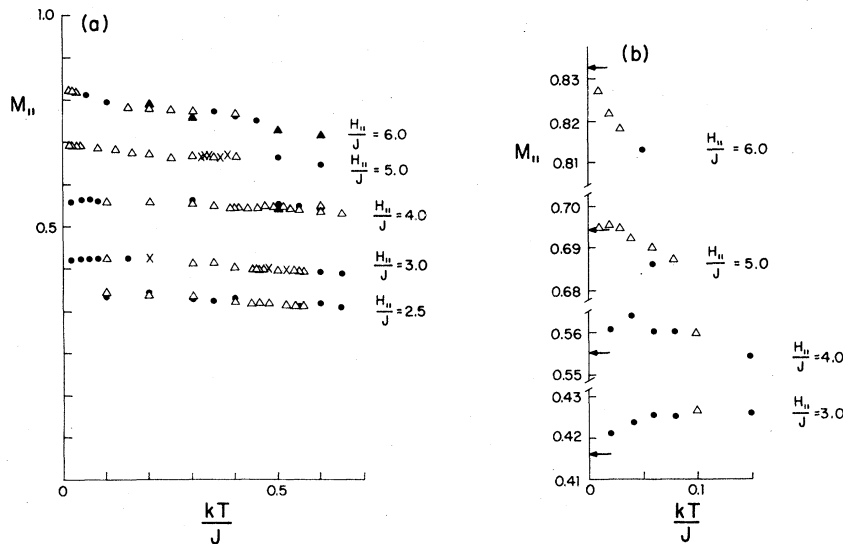


FIG. 10. Temperature dependence of the magnetization for the SF state along paths of constant field. Data are shown for $L = 10$ (Δ); $L = 20$ (\bullet); $L = 40$ (Δ); $L = 100$ (X). The dashed line shown in (a) shows the approximate location of $M_{||}^0$ vs T . The arrows in the high-resolution low-temperature results shown in (b) shows the predictions from the modified harmonic approximation [Eq. (23a)].

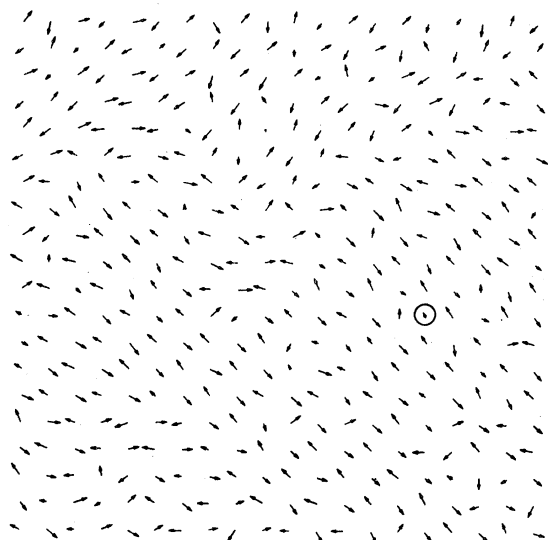


FIG. 11. Projection of spins onto the XY plane for $H_{\parallel}/J=4.0$, and $kT/J=0.3$. Results are for a 20×20 segment of a 40×40 lattice and the circle shows the center of a vortex-antivortex pair.

where 2μ is the energy needed to create a vortex pair. In Fig. 13 we have plotted $\log_{10}\rho$ vs T^{-1} and find that Eq. (29) is valid for the spin-flop state but with a value of 2μ which is field dependent. The modified harmonic approximation model developed in Sec. II relates the behavior of the spin-flop model to that of a plane rotator with modified coupling

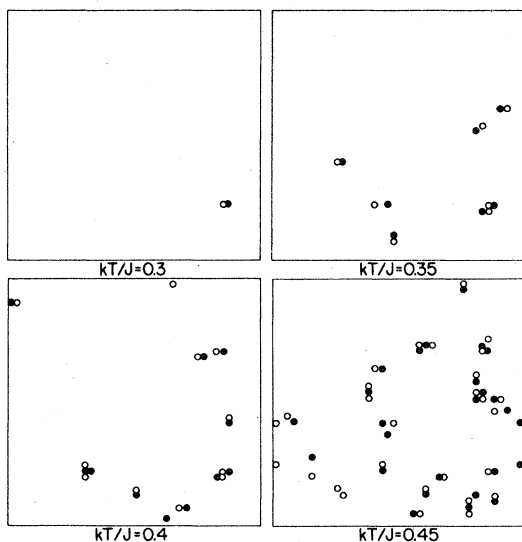


FIG. 12. "Snapshots" of vortex behavior in SF state for $L=40$, $H_{\parallel}/J=4.0$. Open and closed circles depict vortices and antivortices, respectively.

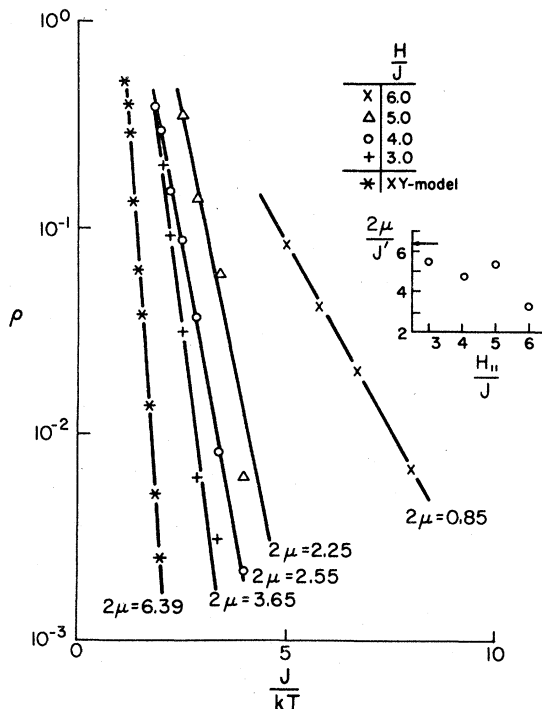


FIG. 13. Vortex-pair density in the SF state. The insert shows the variation of the pair creation energy 2μ normalized by the effective interaction $J' = J(1 - \Delta)[1 - (h/h_{c2})^2]$ (see Sec. II). The arrow shows the pair creation energy for the XY model.

$J' = J(1 - \Delta)[1 - (h/h_{c2})^2]$; hence we have normalized the values of 2μ by dividing by J' . These normalized values, which are shown in the insert in Fig. 13 suggest a slight increase in 2μ with decreasing field. All of these creation energies are much less than the value of $2\mu \sim 10$ estimated for the plane rotator. This is not surprising since the spins in the SF state may simultaneously tip into the $\pm Z$ directions while forming a vortex. This has the effect of reducing the vortex core energy below what would be needed if the spins were constrained to the XY plane. Our results are much closer, however, to the corresponding result which we obtain for the XY model for which reduction of core energy is also possible. The Kosterlitz-Thouless theory¹⁷ predicts that the high-temperature susceptibility diverges as

$$\chi T = A \exp[-b(T - T_c)^{-\nu'}] \tag{30}$$

with $\nu' = 0.5$. In Fig. 14 we test the high-temperature behavior for $H_{\parallel}/J=4.0$ with respect to Eq. (30). The data show extremely pronounced finite size rounding; this observation is consistent with a correlation length which diverges exponentially fast as predicted by theory. For $kT/J \geq 0.5$ the data are well described by Eq. (30) with $b = 1.21$ and $A = 0.23$.

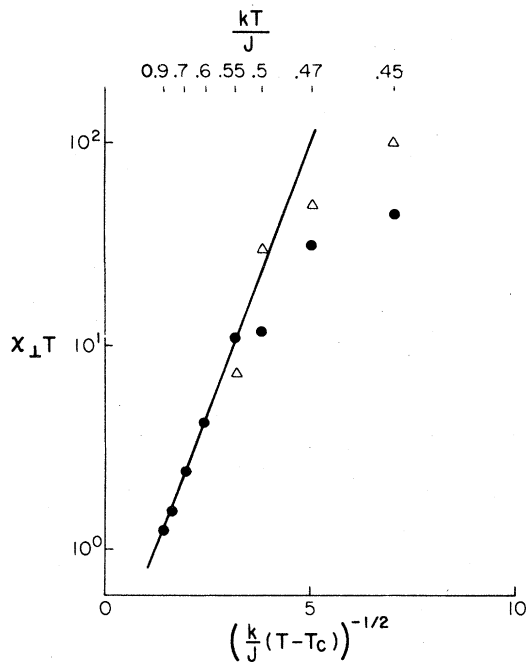


FIG. 14. Behavior of the high-temperature transverse susceptibility for $H_{\parallel}/J=4.0$. Data are shown for $L=20$ (\bullet); $L=40$ (Δ).

3. AF \rightarrow SF transition?

In Fig. 1 we show several possible phase diagrams which show either a first-order AF \rightarrow SF transition or two second-order transitions: AF \rightarrow P followed by P \rightarrow SF. In three dimensions the first possibility was

identified as the correct one based on our observation of relaxation time effects at and near the transition. In Fig. 15 we show magnetization isotherms obtained upon going from the AF to the SF state by increasing the field and by then reducing the field to reenter the AF state. Hysteresis is seen at all four temperatures although it becomes particularly pronounced at low temperatures. By repeating this procedure but with both the number of MCS initially discarded as well as the observation time doubled, we see that the hysteresis loops become narrower. (Upon reentering the AF phase in an $L=20$ lattice at $kT/J=0.1$ we found a metastable biconical state appeared in which one of the sublattices was canted. Here the hysteresis loop did not close up. Data for $L=40$ showed this to be a finite size effect). Relaxation effects were studied for much longer times for $kT/J=0.1$ and the results are shown in Fig. 16. A similar study for the equivalent three-dimensional model³ showed that when we crossed the phase boundary the equilibrium magnetization was reached by a rather distinct two-step process. In contrast the present data show only a very weak shoulder for the AF \rightarrow SF transition and no hint of a step process for the SF \rightarrow AF transition. We interpret these data as supporting the idea of two second-order transitions which lie very close together and which give rise to extremely long relaxation times. We nonetheless cannot exclude the possibility that a biconical tetracritical point occurs but with the biconical phase existing over a very narrow field range. Because of long relaxation times the true equilibrium behavior may be very difficult to observe.

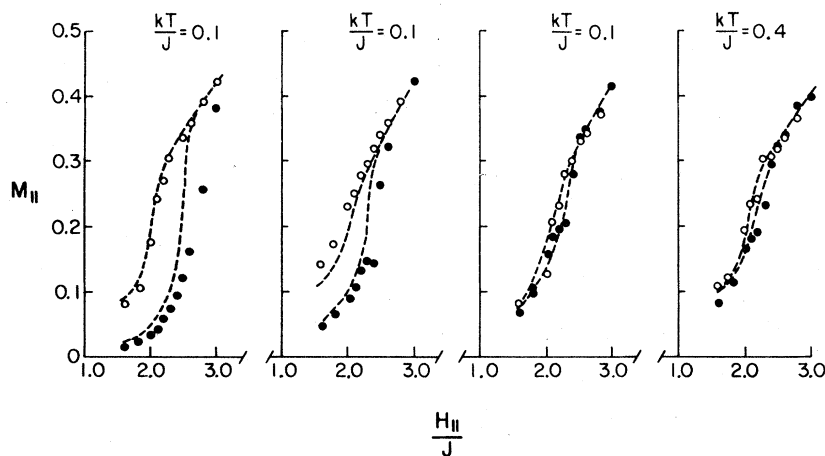


FIG. 15. Field dependence of the magnetization along paths of constant temperature. Data are for $L=20$ with 100 MCS discarded and 50 MCS retained for averages. Closed circles show results obtained for increasing fields and open circles for decreasing fields. The dashed lines show results obtained with 200 MCS discarded and 100 MCS retained for averages.

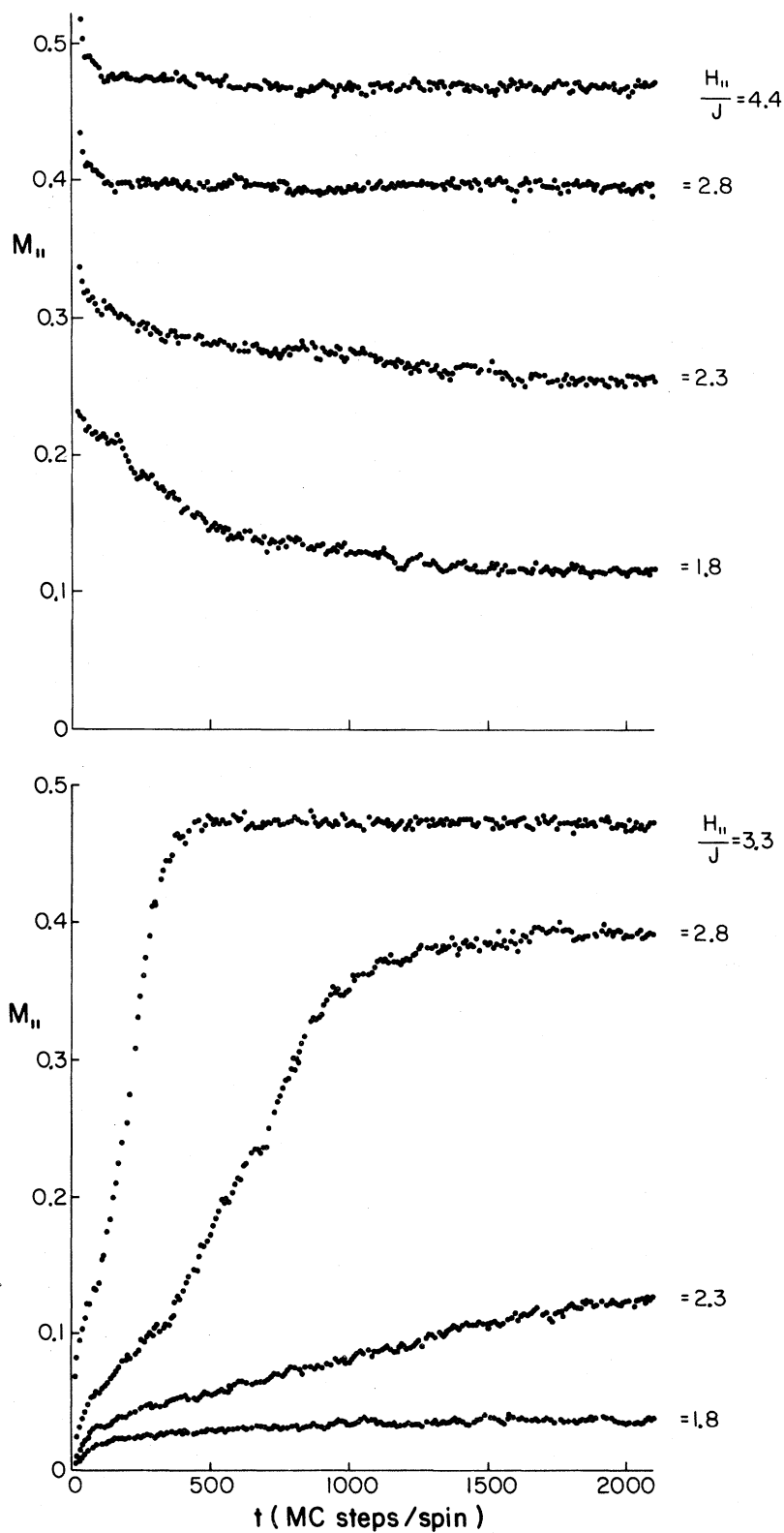


FIG. 16. Relaxation behavior near H_{c1} . Data are for $kT/J=0.1$, $L=40$. Upper diagram—initial state ($t=0$) spin-flop state; lower diagram—initial state antiferromagnetic.

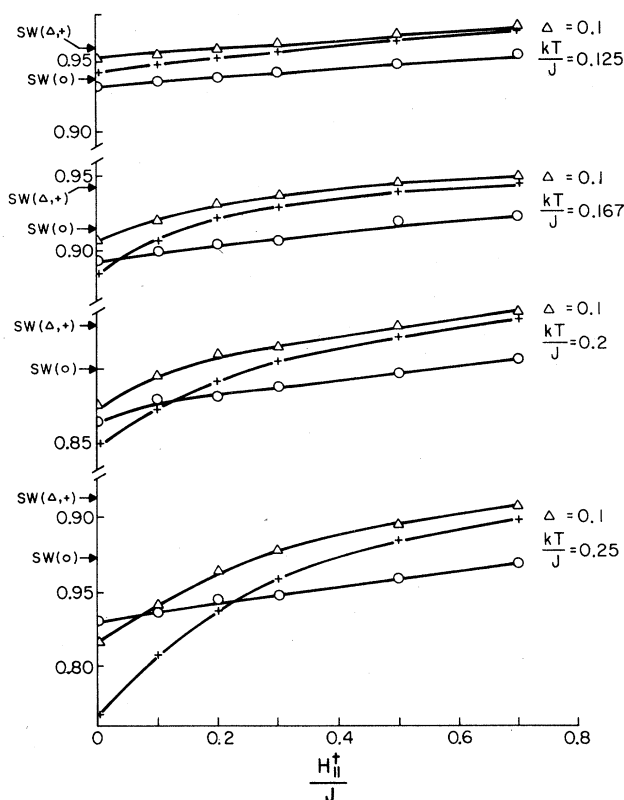


FIG. 17. Reduced energy $\langle E/E_0 \rangle$ (\circ), staggered magnetization m_{\parallel} ($+$), and self-correlation $1 - \langle S_x^2 \rangle$ (∇) plotted vs staggered parallel field H_{\parallel}^{\dagger} . The arrows on the left show zero-field spin-wave predictions.

B. Behavior in a staggered field

We have also studied the low-temperature $H = 0$ response to small nonzero staggered field H_{\parallel}^{\dagger} . The data show that the spin-wave approximation is valid only at extremely low temperatures even for $H = 0$ and that the dependence on H_{\parallel}^{\dagger} is linear only for very low temperature and small H_{\parallel}^{\dagger} (see Fig. 17).

C. Behavior of the XY model in zero field

Since the spin-flop phase of the two-dimensional anisotropic Heisenberg model allows fluctuations in the z component of the spins, a comparison with an XY model might be more appropriate than with a plane rotator model. We have therefore simulated $L = 40$ XY models in zero field to examine both the bulk properties and vortex behavior. The temperature dependence of the internal energy is shown in Fig. 18 in comparison to the corresponding plane rotator results of Tobochnik and Chester.¹⁶ The low-temperature variation is equivalent to a specific heat of $C/R = 1$ as expected from the equipartition

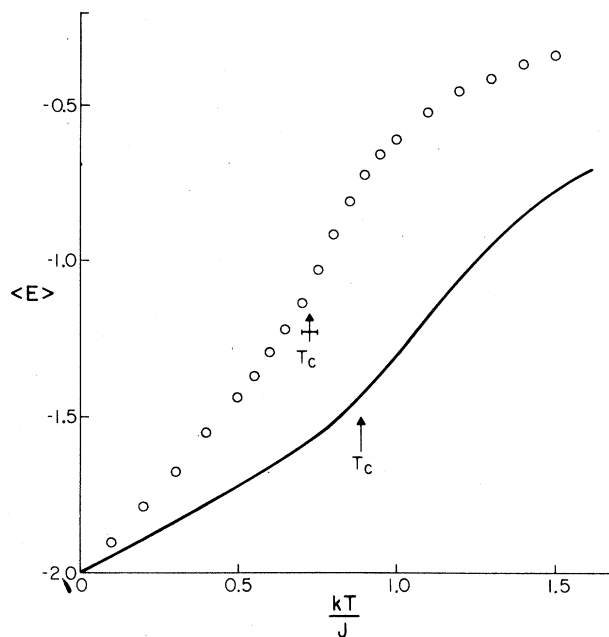


FIG. 18 Temperature dependence of the internal energy of the $L = 40$ XY model. The solid curve shows the corresponding behavior of the two-dimensional plane rotator model (taken from Ref. 16). The arrows show the estimated locations of the critical temperatures.

theorem. (The XY model has one more degree of freedom than the plane rotator). Above $\sim 0.45J$ vortex pairs begin to appear. The increase in the density of vortex pairs is well described by Eq. (29) (see Fig. 13), but with a formation energy of $2\mu = 6.39$ as compared with the plane rotator value of $2\mu \sim 10$. From the unbinding of the vortex pairs we estimate that $kT_c/J \sim 0.725 \pm 0.025$. Additional excitations can appear in the XY model which are not present in the plane rotator. (For example, as mentioned earlier the core energy of the vortices can be reduced by simply tilting all spins out of the XY plane.) In Fig. 19 we compare the high-temperature susceptibility of the XY model to that found for the plane rotator. Because of the large finite size rounding in both cases, an accurate determination of the critical temperatures is quite difficult to obtain. We have adopted the predicted Kosterlitz-Thouless form [Eq. (30)] for displaying the data. [Fits to data over a moderately restricted temperature range have suggested that the power of $(T - T_c)$ in Eq. (30) might be different from $-\frac{1}{2}$. Although we have chosen to analyze the data on both models in the same fashion, we refer the reader to the original work on the plane rotator for a more detailed analysis.] We find that the XY-model susceptibility is well described by the Kosterlitz-Thouless prediction with $A = 0.40$, $b = 1.55$. Our simple fit for the plane rotator yields an almost identical amplitude, $A = 0.42$ and $b = 2.56$.

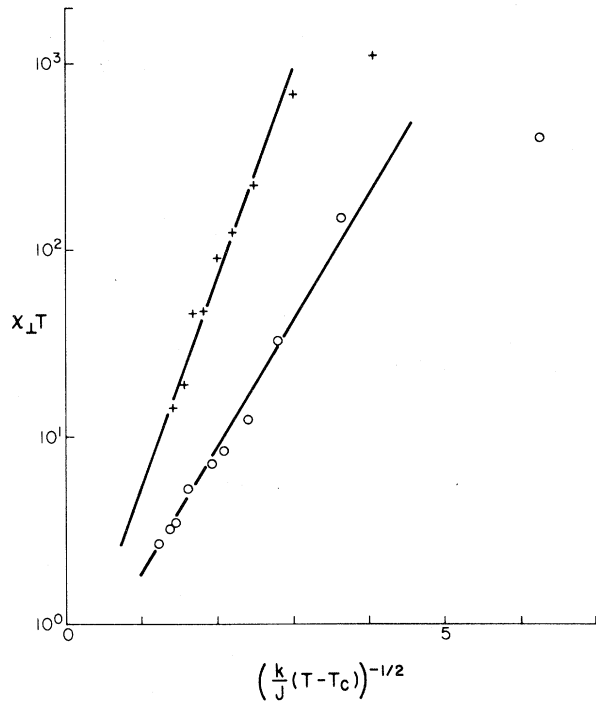


FIG. 19. Temperature dependence of the high-temperature transverse susceptibility $\chi_{\perp T}$ for $L = 60$ plane rotator (+) (taken from Ref. 16); and for an $L = 40$ XY model (O). The data are plotted using $kT_c/J = 0.9$ for the plane rotator and $kT_c/J = 0.725$ for the XY model.

Although the qualitative features of the XY model and plane rotator transitions are the same, it is therefore not surprising that quantitative differences do occur.

D. Behavior of the isotropic Heisenberg antiferromagnet in a uniform field

We have also studied the behavior of the isotropic ($\Delta = 0$) antiferromagnet in uniform fields between $H/J = 0.01$ and 7.0 . This is a model which has a bicritical point (at $H = 0$) which is of strictly isotropic Heisenberg character. The character of the bicritical behavior changes when $\Delta \rightarrow 0$ since the AF phase disappears but the SF phase stays the same. In all cases vortex behavior was observed which was qualitatively identical to that seen in the XY model and $\Delta = 0.2$ SF phase. From the vortex-pair unbinding we have estimated the transition temperatures plotted in Fig. 20. The results for $H/J = 0.01$ indicate that $T_c(H)$ approaches zero extremely slowly as $H \rightarrow 0$. In Fig. 21 we show the temperature dependence of the vortex-pair density. The normalized values of vortex-pair formation energy $2\mu/J'$ show a definite maximum as a function of H and then decreases

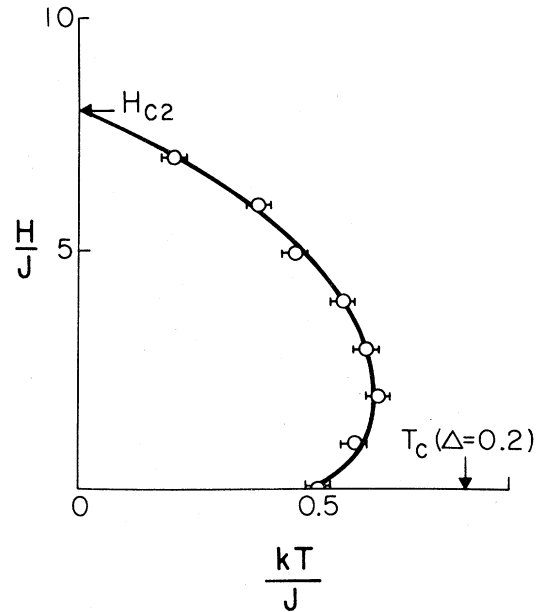


FIG. 20. Phase boundary for the isotropic ($\Delta = 0$) Heisenberg antiferromagnet in a uniform magnetic field.

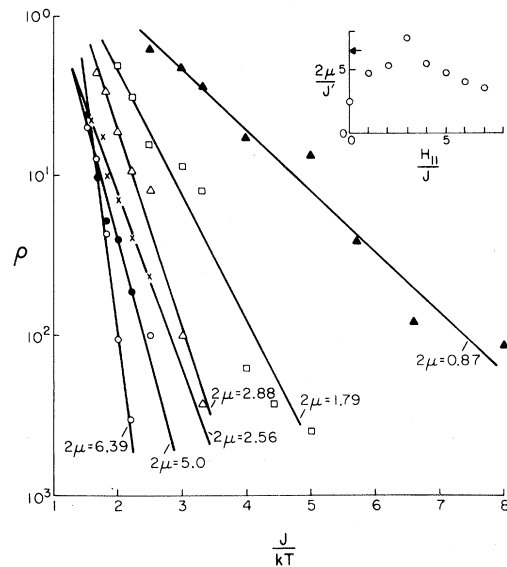


FIG. 21. Temperature dependence of the vortex-pair density for the isotropic ($\Delta = 0$) Heisenberg antiferromagnet in a uniform field. The insert shows the variation of the pair creation energy 2μ normalized by the effective interaction $J' = J[1 - (h/h_c)^2]$ (see Sec. II). The arrow shows the pair creation energy for the XY model.

dramatically as $H \rightarrow 0$. A comparison of Fig. 21 and Fig. 13 shows that the dependence of $2\mu/J'$ on H/H_{c2} is quite similar.

V. CONCLUSIONS

The behavior of a simple model Hamiltonian for classical two-dimensional anisotropic Heisenberg antiferromagnets has been investigated by extensive Monte Carlo computer simulations. We find a low-field AF phase with Ising-like critical exponents. The low-temperature properties of this phase are described by first-order spin-wave theory but deviations become important at extremely low temperatures. The SF state shows behavior which is generally described by the Kosterlitz-Thouless for the two-dimensional planar model. We find no long-range order but instead vortex-pair excitations involving the transverse spin components. We have developed a harmonic approximation theory which maps the SF phase onto the plane rotator theory of Berezinski. We find that this approach is unsatisfactory and attribute its deficiencies to the neglect of fluctuations in the z components of spin. This is borne out by simu-

lations on the XY model. The nature of the transition between the AF and SF phases is still unclear. Our data show a distinct umbilicus but we cannot exclude the possibility that it terminates at a biconical tetracritical point instead of a bicritical point. For comparison, we have carried out studies on the field induced SF state in the isotropic Heisenberg model including near the $H = 0$ bicritical point. The SF phase in this model is similar to that in the anisotropic antiferromagnet. The transition temperature approaches zero *very* slowly and the vortex-pair creation energy also decreases as the field approaches zero. A more definitive description of the "spin-flop line" will require extremely long simulations on quite large lattices and will be reported later.

ACKNOWLEDGMENTS

This research was supported in part by NATO Grant No. 1185 and by the National Science Foundation. One of us (D.P.L.) also wishes to thank the Kernforschungsanlage Jülich for its hospitality during a portion of the time during which this research was carried out.

¹M. E. Fisher, in *Magnetism and Magnetic Materials—1974*, edited by C. D. Graham, G. H. Lander, and J. J. Rhyne, AIP Conf. Proc. No. 24 (AIP, New York, 1975), p. 273.

²J. M. Kosterlitz, D. R. Nelson, and M. E. Fisher, *Phys. Rev. B* **13**, 412 (1976).

³D. P. Landau and K. Binder, *Phys. Rev. B* **17**, 2328 (1978).

⁴C. J. Gorter and T. van Peski-Tinbergen, *Physica (Utrecht)* **22**, 273 (1956).

⁵H. Rohrer and H. Thomas, *J. Appl. Phys.* **40**, 1025 (1969).

⁶K. W. Blazey, H. Rohrer, and R. Webster, *Phys. Rev. B* **4**, 2287 (1971).

⁷M. E. Fisher and D. R. Nelson, *Phys. Rev. Lett.* **32**, 1634 (1975).

⁸M. E. Fisher, *Phys. Rev. Lett.* **34**, 1634 (1975).

⁹D. R. Nelson, J. M. Kosterlitz, and M. E. Fisher, *Phys. Rev. Lett.* **33**, 813 (1974).

¹⁰N. D. Mermin and H. Wagner, *Phys. Rev. Lett.* **17**, 1133 (1966).

¹¹F. S. Rys, in *Magnetism and Magnetic Materials—1975*, edited by J. J. Becker, G. H. Lander, and J. J. Rhyne, AIP Conf. Proc. No. 29 (AIP, New York, 1976), p. 458.

¹²V. L. Berezinskii, *Zh. Eksp. Teor. Fiz.* **59**, 907 (1970) [*Sov. Phys. JETP* **32**, 493 (1971)]; **61**, 1144 (1971) [**34**, 610 (1972)]; see also V. L. Berezinskii and A. Ya. Blank, *ibid.* **64**, 725 (1973) [**37**, 369 (1973)].

¹³K. Binder and H. Rauch, *Z. Phys.* **219**, 201 (1969).

¹⁴K. Binder and D. P. Landau, *Phys. Rev. B* **13**, 1140 (1976).

¹⁵D. J. Thouless (private communication).

¹⁶J. Tobochnik and G. V. Chester, *Phys. Rev. B* **20**, 3761 (1979).

¹⁷J. M. Kosterlitz and D. J. Thouless, *J. Phys. C* **6**, 1181 (1973).